

Cross-Species and Cross-Modality Epileptic Seizure Detection via Multi-Space Alignment

Ziwei Wang^{1,2}, Siyang Li^{1,2} and Dongrui Wu^{1,2,*}

ABSTRACT

Epilepsy significantly impacts global health, affecting about 65 million people worldwide, along with various animal species. The diagnostic processes of epilepsy are often hindered by the transient and unpredictable nature of seizures. Here we propose a multi-space alignment approach based on cross-species and cross-modality electroencephalogram (EEG) data to enhance the detection capabilities and understanding of epileptic seizures. By employing deep learning techniques, including domain adaptation and knowledge distillation, our framework aligns cross-species and cross-modality EEG signals to enhance the detection capability beyond traditional within-species and with-modality models. Experiments on multiple surface and intracranial EEG datasets of humans and canines demonstrated substantial improvements in the detection accuracy, achieving over 90% AUC scores for cross-species and cross-modality seizure detection with extremely limited labeled data from the target species/modality. To our knowledge, this is the first study that demonstrates the effectiveness of integrating heterogeneous data from different species and modalities to improve EEG-based seizure detection performance. The approach may also be generalizable to different brain-computer interface paradigms, and suggests the possibility to combine data from different species/modalities to increase the amount of training data for large EEG models.

Keywords: Electroencephalogram, Automatic Seizure Detection, Transfer Learning, Domain Adaptation, Knowledge Distillation

INTRODUCTION

Epilepsy is a chronic disorder characterized by sudden abnormal neuronal discharges, resulting in transient brain dysfunction [1]. It affects approximately 1% of the population (65 million) worldwide, including adults, infants, and young children, and is highly prevalent among various animal species as well [1–3]. Epileptic individuals exhibit a range of symptoms [4], including generalized convulsions, loss of consciousness, debilitation, and recurrent seizures. These symptoms may cause irreversible brain damage and life-threatening situations [5], which can lead to employment restrictions and social isolation.

Consequently, early diagnosis and preventative measures for epilepsy are of paramount importance. Sophisticated medical imaging modalities such as computed tomography and magnetic resonance imaging enable epilepsy detection by identifying lesions and providing com-

prehensive spatial information [6]. However, these techniques lack temporal resolution and cannot capture ongoing seizures. To overcome these limitations and facilitate timely epilepsy diagnosis, electroencephalogram (EEG) signals are utilized for their high temporal resolution.

EEG provides a diagnostic test that detects epileptiform discharges by monitoring voltage fluctuations caused by neural activities of the brain [7]. EEG can be further categorized into scalp EEG (sEEG) and intracranial EEG (iEEG) based on the signal acquisition location. While sEEG is readily available and non-invasive, it is more prone to artifacts caused by electrode shifts, muscle movements, volume conduction effects, etc [8]. In contrast, iEEG offers superior signal-to-noise ratio and sensitivity, as it directly targets specific brain areas and samples from deep brain regions inaccessible to scalp electrodes, at the cost of requiring brain surgery [3].

¹Ministry of Education Key Laboratory of Image Processing and Intelligent Control, School of Artificial Intelligence and Automation, Huazhong University of Science and Technology, Wuhan 430074, China; ²Shenzhen Huazhong University of Science and Technology Research Institute, Shenzhen 518000, China.

*Corresponding author.
Email: drwu09@gmail.com.

Received: XX XX Year;
Revised: XX XX Year;
Accepted: XX XX Year

Accurate decoding of epileptic EEG signals is crucial for aiding medical diagnosis, assisting neurologists in treatment, and reducing the risk of seizures [7]. Although EEG-based seizure detection has achieved significant progresses, these advances have imposed a considerable burden on physicians, requiring them to visually scrutinize up to several days of EEG signals to identify abnormal electrical discharges [9]. Such manual analysis is time-consuming and heavily expert-dependent, driving the recent development of automated algorithms for EEG-based epilepsy detection.

Previous studies involving traditional feature-based machine learning algorithms [10–12] and deep learning algorithms [13–15] have been widely explored for automatic epilepsy detection. Most works in the literature focus on within-patient seizure classification [13–15], in which the training and test sets typically originate from the same group of patients. However, such within-patient analysis could not be directly applied to unseen patients due to significant non-stationarity and individual differences of EEG signals [16]. Consequently, researchers have started investigating cross-patient seizure detection, utilizing auxiliary patient’s labeled data to relieve the reliance on target patient’s labeled data [16–18]. However, both within-patient and cross-patient seizure detection require an adequate amount of labeled data from the human patients for effective model training, which may not always be available.

To solve the above challenge, we propose to harness existing data from other species and build a cross-species and cross-modality transfer learning framework for epilepsy seizure detection. A few prior works delineated below have explored the correlations of epilepsy of humans and other species, through the lens of biological mechanisms.

Several biological models have been shown to possess cross-species applicability [19]. Many neurological and psychiatric disorders impact both humans and animals. Advances in diagnostics and therapeutics in human neurology and psychiatry are often translatable to veterinary patients, and vice versa. For instance, photosensitive generalized seizures in baboons provide insights into similar seizures in humans [20]. Lipid accumulation in the brain is a significant pathological feature of epilepsy in both humans and mice [19]. Human ischemic stroke gene expression biomarkers can be obtained from rat brain samples [21]. Similar patterns and evolutions of epileptiform discharges are observed in both hu-

man and mouse brains [22].

Structural and functional elements of biological systems are shared among vertebrates [20]. Canine epilepsy shares many characteristics with human epilepsy [23], including periodic features [3], energy features, and temporal morphology, as illustrated in Figures 1 a-c. Previous works have shown that human drugs such as levetiracetam and gabapentin are of benefit to dogs with refractory epilepsy [24], and naturally occurring canine epilepsy offers a potential biological model of human epilepsy [25]. Cross-species approaches to brain research can utilize prior knowledge from other species to enhance the understanding of diseases in the current species [20].

We aim to utilize cross-species and cross-modality epileptic EEG signals to increase the amount of training data, investigate the common characteristics of epileptic signals across species and modalities, and facilitate knowledge transfer. We demonstrate that EEG data from one species/modality can enhance the seizure detection performance of another species/modality, suggesting the potential of integrating data from different species and modalities to improve EEG decoding performance. The proposed cross-species and cross-modality epilepsy seizure detection framework is shown in Figure A1a. The deep neural network model is trained on canine iEEG signals and subsequently tested on human iEEG/sEEG signals, achieving a transfer from canines to humans. Likewise, the transfer from humans to canines is also achievable.

Importantly, disparities exist in the EEG signals across species that must be appropriately addressed to achieve optimal transfer performance, which is the core problem we aim to solve in this work. EEG signals of different species are collected from varying numbers of electrodes, using different sampling rates and diverse collection devices, as illustrated in Figure 1d. These result in distinct signal characteristics. For instance, human iEEG signals could be sampled from various subdural electrode grids based on individual clinical considerations; the number of electrodes could go as many as 72, whereas canine iEEG signals may be acquired from an implanted device with 16 subdural electrodes [26]. In another example, the human iEEG signals were collected from three focal and three extra-focal electrodes [27], whereas sEEG signals were collected via scalp electrodes [16,28]. These discrepancies complicate the cross-species transfer of feature heterogeneity. A naïve solution would be to discard the additional electrodes, result-

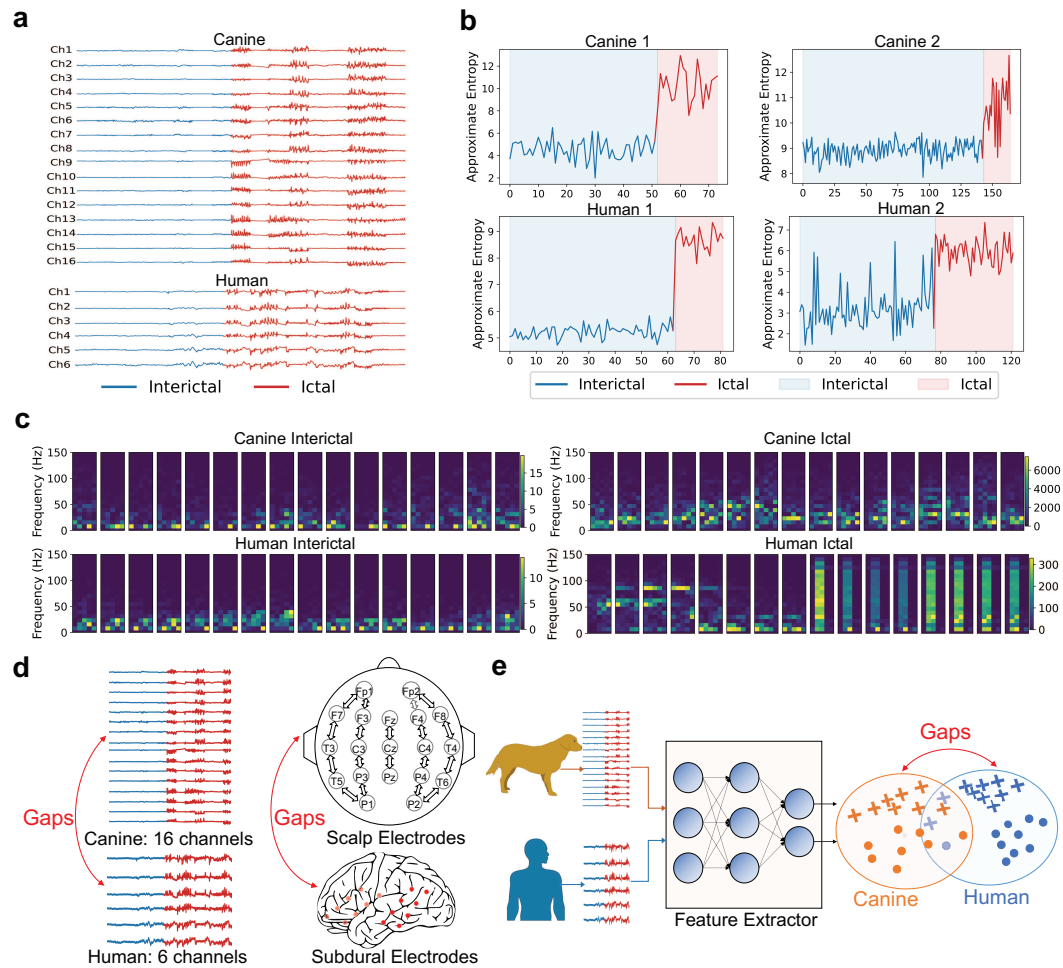


Figure 1. Evidences for cross-species and cross-modality feature transferability, along with gaps for successful knowledge transfer in algorithm design. **a**, iEEG from both canines and humans exhibits large fluctuations during epileptic seizures, indicating the transferability of time-domain features across species. **b**, The approximate entropy of iEEG from both species increases significantly during seizures, indicating the transferability of entropy features across species. **c**, Power spectral density spectrograms, derived from consecutive Fourier transforms for both species, show an increase in the power across all channels during seizures, suggesting the transferability of frequency-domain features. **d**, Input space disparity across species are highlighted by the discrepancy in electrode configurations between species. Sixteen intracranial electrodes were used for canines iEEG data collection in the Kaggle dataset, whereas only six were used for humans iEEG data collection in the Freiburg dataset. Canine iEEG signals were captured using intracranial electrodes linked to implanted devices, whereas human sEEG signals in the NICU and CHSZ datasets were collected via scalp electrodes, demonstrating the configuration differences. **e**, Feature distribution gaps between canines and humans.

ing in the loss of valuable information. Even if the data are perfectly normalized in the input space, the extracted features may still exhibit significant distribution shifts, as illustrated in Figure 1e. Such problems have caused considerable difficulty in algorithm design for cross-species and cross-modality transfer.

To minimize cross-species and cross-modality discrepancies and enhance the transfer performance, we implemented alignments simultaneously in the input, feature and output spaces, eliminating the gaps of channel heterogeneity, distribution shifts, and prediction inconsistency. The details are illustrated in Figure A1 of Appendix A.

Utilizing cross-species and cross-modality data could enhance the decoding of EEG signals for species with limited available data. Additionally, merging EEG datasets from different species and modalities can substantially increase the quantity of the training set, providing adequate training data for deep learning models or large-scale models. By exploring methods to mitigate data distribution discrepancies between species and modalities, we can also bridge inter-species and inter-modality gaps and offer novel insights for clinical endeavors.

RESULTS AND ANALYSIS

Datasets introduction

We aim to simulate realistic clinic settings where the target species in consideration provides little or no labeled data, and labeled data have to be obtained from auxiliary species to build accurate decoding algorithms. Such auxiliary datasets may have very distinct characteristics, including the number of channels, sampling rates, discrepancies in intracranial or scalp electrode placements, etc.

Four public epileptic seizure datasets were employed in this study: the Kaggle dataset from the Kaggle UPenn and Mayo Clinic’s Seizure Detection Challenge [26]; the Freiburg dataset from the Epilepsy Center of the University Hospital of Freiburg, Germany [27]; the CHSZ dataset from Wuhan Children’s Hospital, Tongji Medical College, Huazhong University of Science and Technology, China [16]; and, the NICU dataset from Helsinki University Hospital’s neonatal intensive care unit [28]. More details about the datasets can be found in Appendix B, and the data preprocessing procedures are outlined in Appendix C.

Transfer tasks and scenarios

We considered both canine-to-human transfer and human-to-canine transfer tasks:

1. Canine-to-human: Train the model using iEEG data from canines, and test on human iEEG/sEEG data.
2. Human-to-canine: Train the model using iEEG/sEEG data from humans, and test on canine iEEG data.

Depending on whether the test species of interest has any labeled data, two cross-species transfer scenarios were experimented:

1. Unsupervised cross-species transfer: The training data are exclusively from another species, and data from the target species are utilized for testing. This is a typical unsupervised transfer learning scenario, with different species representing distinct domains.
2. Semi-supervised cross-species transfer: A small amount of labeled data from one subject in the target species is combined with all data from another species to train the model, with the remaining target data used for testing. This is a semi-supervised transfer learning scenario. For all datasets, the proportion of labeled trials per class for each subject increased from 5% to 20% with a step of 5%.

In the unsupervised cross-species transfer scenario, models were trained on auxiliary species’ labeled data and tested on each subject of the target species, with the average classification scores across all target patients computed as the final result. In the semi-supervised cross-species transfer scenario, models were trained on auxiliary species’ labeled data in combination with labeled data from a target subject, and tested on the remaining test data of the target subject, then averaged over all test subjects.

The Area Under the Receiver Operating Characteristic curve (AUC) metric was used as the performance measure. Compared with raw accuracy score, precision, or recall, the AUC is a better metric that evaluates a model’s ability to discriminate between seizure and non-seizure clips, regardless of the specific classification threshold selected.

Transfer learning approaches

Euclidean Alignment (EA) [29] was used as a standard preprocessing step on the two iEEG datasets to address the heterogeneities in electrode placements across subjects. EA standardizes iEEG data by aligning the mean covariance matrices of all iEEG trials for each subject in-

dividually, ensuring consistency across all subjects.

Domain adaptation [30] aims to enhance data distribution matching by integrating labeled source data with unlabeled target data. Five popular unsupervised domain adaptation approaches introduced in Appendix A were compared without the proposed ResizeNet introduced in Figure A1b, and the number of channels for both species was unified by eliminating the mismatching channels.

Knowledge distillation [31] facilitates the transfer of knowledge from a more sophisticated model (teacher) to a simpler one (student). This process utilizes the Kullback-Leibler (KL) divergence to align the probability distributions of both models' outputs, ensuring similar predictive behaviors. Our approach incorporates channel-wise knowledge distillation to refine this alignment, depicted in more details in Methods and Figure A1c. Six popular knowledge distillation approaches introduced in Appendix A were combined with the proposed ResizeNet to further improve the alignment performance.

We denote the proposed multi-space alignment approach as ResizeNet+MSA, which simultaneously performs input, feature, and output space alignments to handle channel disparity and distribution shifts for cross-species and cross-modality transfer.

Results

The unsupervised cross-species and/or cross-modality transfer learning results are shown in Table 1, the semi-supervised cross-species and within-modality transfer learning results are shown in Table 2, and the semi-supervised cross-species and cross-modality transfer learning results are shown in Table 3.

Automatic epileptic seizure detection using cross-species and/or cross-modality deep learning achieves promising performance For the two iEEG datasets (Kaggle and Freiburg), over 90% AUC can be achieved with a minimum amount of target patient labeled data (as low as only 5%), as shown in Tables 2 and 3. For the two sEEG datasets, transferring from humans to canines can also reach over 90% AUC with 10% target canine labeled data.

Utilizing cross-species auxiliary labeled data is beneficial Within-species models for seizure detection consistently under-performed models utilizing cross-species auxiliary labeled data. Within-species analysis highly relies on species-specific data and is impossible to perform in scenarios shown in Table 1, since there are no la-

beled data from the target species. Even in scenarios shown in Tables 2 and 3, it is always beneficial to utilize auxiliary labeled data from another species, regardless of which specific algorithm was used. The results highlight the critical role of utilizing additional larger labeled training data in enhancing model generalizability and accuracy. Particularly, models trained exclusively within the same species failed to capture the broader phenotypic variations of epilepsy, which were effectively modeled by incorporating cross-species data, thus leveraging the generalized neurological patterns observed across different species.

Our multi-space alignment framework is much more effective than all standalone strategies The multi-space alignment framework, encompassing simultaneously input, feature, and output space alignments, demonstrating superior performance over all standalone strategies. As shown in the ablation study results in Figure 2a, performing alignments in more spaces generally resulted in higher AUCs.

Figure 2b shows t -distributed stochastic neighbor embedding (t -SNE) visualizations [32] of iEEG features from canines and humans of the Kaggle dataset. In the two-dimensional reduced feature space, the distribution of raw iEEG data from different species exhibited clear distinctions (Baseline). However, following alignment by EA, domain adaptation, or knowledge distillation, the distributions became similar, with class separability significantly enhanced (different colors of the same shape merged).

We conducted hyperparameter sensitivity analysis to further investigate the impact of the two weights in Eq. (6), i.e., λ for the knowledge distillation loss and β for the domain adaptation loss. All experiments were repeated three times, and the results are shown in Figure 2c. The proposed ResizeNet with knowledge distillation loss was robust over a wide range of λ and β values.

Cross-species and cross-modality feature heterogeneity can be accommodated by ResizeNet projection and knowledge distillation The integration of ResizeNet and knowledge distillation addresses the cross-species and cross-modality feature heterogeneity effectively. ResizeNet's ability to project and transform features into a unified space, coupled with knowledge distillation's ability in refining and transferring essential information, proved crucial. As shown in Tables 1-3, ResizeNet almost always outperformed Baseline approaches which brutally match the channels by truncation. Re-

sizeNet ensured that the entire feature space pertinent to seizure detection was preserved and accurately interpreted across species, resulting in significant detection performance improvement. Our proposed ResizeNet+MSA almost always achieved the best performance.

To visualize the impact of the proposed approach, Figure 3a plots the iEEG/sEEG trials before and after input space alignment via the proposed ResizeNet in the time domain, and Figure 3b plots their approximate entropy. iEEG/sEEG signals before and after ResizeNet exhibit similar temporal structures and entropy features, demonstrating the effectiveness of ResizeNet in maintaining the key information while unifying signal forms across species.

EA is pivotal and a must-have for data normalization in all transfer learning tasks EA proved to be essential in data normalization in cross-species and cross-modality transfers, addressing significant discrepancies in EEG data distributions. As shown in Figure 2a, the performance gain by using EA was tremendous. By aligning the data to a common scale, we effectively mitigated the discrepancies in the input space, which are crucial for subsequent machine learning. EA has been shown to be effective in various cross-subject transfer tasks [33,34], and this work shows that EA is also beneficial to cross-species and cross-modality transfers.

Domain adaptation helps feature distribution alignment in cross-species and cross-modality transfers Domain adaptation aligns the feature distributions between species and modalities, significantly improving the transferability of seizure detection models, as shown in Tables 1-3. By reducing the probability distribution gap, common and transferable features may be easily revealed.

Our transfer learning framework significantly reduces expert labeling efforts Our framework reduces the need for extensive expert labeling, which is a significant bottleneck in traditional EEG analysis for epilepsy seizure detection. Note that expert labeling for target patients is still of critical importance regardless of whether there exists auxiliary labeled data from other species and/or modalities: ResizeNet+MSA works better with a small portion of labeled data from the target subject than without any, e.g., results from semi-supervised cross-species transfer in Tables 2-3 are much better than those in unsupervised cross-species transfer in Table 1. Our approach cannot completely eliminate the need for expert labeling, but greatly reduces the amount of labeled target data

to reach a specific accuracy. For example, as shown in Tables 2-3, cross-species transfer using ResizeNet+MSA with 5% target labeled data generally outperformed within-species analysis of over 20% labeled data.

DISCUSSION

This study introduces a novel cross-species and cross-modality framework for epileptic seizure detection using EEG data. Through multi-space alignment, we have developed a framework that not only addresses the fundamental challenges of EEG data variability across species and modalities, but also enhances the generalizability and accuracy of seizure detection.

Broad implications

To our knowledge, this is the first study that demonstrates the effectiveness of integrating heterogeneous data from different species and modalities to improve EEG-based seizure detection performance. However, the implications of this research extend beyond improving epilepsy diagnostics. The cross-species and cross-modality framework could revolutionize how neurological disorders are studied and treated, offering a model for developing diagnostic tools that are more broadly applicable. For clinical practice, this means diagnosis for populations where traditional approaches are incapable may be performed.

Our approach may also be generalizable to different brain-computer interface paradigms [33,35], and suggests the possibility to combine data from different species/modalities to increase the amount of training data for large EEG models.

Limitations and future research

Despite the promising performance, several limitations must be addressed in future research.

The diversity of EEG acquisition protocols and hardware configurations across different clinical and research settings introduces variability that complicates data standardization and model training. Establishing universal protocols for EEG data collection and preprocessing could enhance the reproducibility of our findings and facilitate wider adoption of the technology.

The current study primarily focuses on iEEG/sEEG data from canines and humans. Expanding this research to include other species and modalities (e.g., magnetoencephalography)

Table 1. Average unsupervised cross-species and/or cross-modality transfer AUCs (%) on the four datasets. The best average AUC of each task is marked in bold, and the second best by an underline.

Approach		Canine-to-Human ¹					Human-to-Canine ²				
		Kaggle (iEEG -to- iEEG)	CHSZ (iEEG -to- sEEG)	NICU (iEEG -to- sEEG)	Freiburg (iEEG -to- iEEG)	Avg.	Kaggle (iEEG -to- iEEG)	CHSZ (sEEG -to- iEEG)	NICU (sEEG -to- iEEG)	Freiburg (iEEG -to- iEEG)	Avg.
Baseline ³	Source Only ⁵	68.43±1.0	75.00±2.7	62.87±0.9	60.97±0.5	66.82	73.09±1.1	71.15±2.5	53.26±4.9	75.72±1.8	68.31
	DAN	75.91±0.4	78.46±0.5	68.76±0.1	60.91±0.7	71.01	73.69±0.4	74.77±1.5	66.56±4.2	75.84±0.5	72.72
	JAN	75.47±1.1	79.53±1.6	67.99±1.6	60.95±1.1	70.99	73.66±0.4	76.44±1.3	60.73±2.8	74.76±1.0	71.40
	SHOT	76.82±0.2	68.16±2.1	<u>69.72</u> ±0.5	59.70±1.0	68.60	73.93±0.6	58.05±2.1	51.75±0.5	66.64±2.9	62.59
	DSAN	<u>77.79</u> ±1.9	67.48±5.5	67.03±0.8	61.16±0.7	68.37	73.71±1.2	78.14±1.1	59.07±5.1	75.00±0.6	71.48
	MCC	76.71±1.3	71.91±2.0	69.54±0.9	61.72±0.9	69.97	75.05±0.3	56.97±1.6	53.64±2.8	72.08±2.0	64.44
ResizeNet+ ⁴	AT	70.75±1.9	79.31±3.2	68.71±2.2	61.00±2.1	69.94	75.44±0.2	77.27±3.7	<u>66.68</u> ±4.5	74.04±1.2	<u>73.36</u>
	NST	73.98±4.9	74.74±1.5	66.22±1.4	63.94 ±0.7	69.72	74.78±1.7	<u>79.36</u> ±1.1	61.82±6.6	75.75±1.2	72.93
	SP	74.05±5.2	78.14±4.0	68.51±2.6	<u>63.59</u> ±1.1	<u>71.07</u>	75.08±0.5	78.07±3.3	60.30±1.6	73.93±0.3	71.85
	RKD	77.78±1.0	78.70±2.9	65.93±1.5	61.39±0.8	70.96	75.31±0.4	76.17±3.5	59.53±2.7	75.71±1.9	71.68
	PKT	71.30±3.5	<u>79.94</u> ±2.1	68.51±1.6	63.49±1.2	70.81	<u>75.47</u> ±0.8	77.80±3.1	61.03±1.7	<u>75.85</u> ±2.1	72.54
	CC	71.67±0.6	79.15±0.7	68.98±1.9	57.20±2.8	69.25	74.50±1.6	76.09±0.9	65.88±2.2	75.15±1.0	72.91
	MSA (ours)	85.41 ±1.2	82.23 ±0.8	72.42 ±1.2	62.05±0.6	75.53	77.93 ±1.0	80.70 ±0.6	72.10 ±1.6	76.83 ±1.6	76.89

¹ Canine-to-Human: Train on iEEG data from four canines in the Kaggle dataset, and test on a human iEEG/sEEG dataset.

² Human-to-Canine: Train on a human iEEG/sEEG dataset, and test on iEEG data from four canines in the Kaggle dataset.

³ Baseline: Without using the proposed ResizeNet, the number of channels for both species is unified by eliminating the mismatching ones.

⁴ ResizeNet+: Utilize the proposed ResizeNet projection to unify the number of channels for different species and/or modalities.

⁵ Source Only: Train the model on all labeled data from the other species without employing any alignment strategy.

could provide deeper insights into the neurological underpinnings of seizures and other related disorders.

Finally, merging multiple auxiliary datasets is also worth exploring. In the proposed cross-species epilepsy detection framework, the training set consists of one dataset from another species (and a small amount of data from the target species in the semi-supervised cross-species and cross-modality transfer scenario). However, in practice, multiple datasets could be utilized to augment the training set. For instance, a model can be trained on a combination of several human datasets and subsequently tested on the canine dataset.

METHODS

Disparity in data characteristics poses a significant challenge in real-world machine learning applications, particularly in EEG-based seizure detection. In cross-species seizure detection, where different species represent distinct domains, the source and target species often differ significantly in aspects such as seizure subtype, location, duration, and signal collection device. These variations introduce discrepancies across input, feature, and output spaces, compounded

by individual differences and configuration discrepancies arising from diverse EEG equipment and protocols. For instance, the canine iEEG data in Kaggle used 16 channels, whereas the human iEEG data used 16 to 72 channels with varying sampling rates. Accommodating these discrepancies is crucial for optimal cross-species transfer performance.

We introduce our multi-space alignment approach below.

Input space normalization

Inter-species variability leads to significant discrepancies in the marginal probability distributions of EEG signals. Euclidean Alignment (EA) [29] has been demonstrated to be effective in EEG-based classification tasks like motor imagery. This unsupervised approach aligns EEG data from different patients within the same species and across species, making subsequent analyses easier and more robust.

We apply EA to each subject separately to mitigate individual differences, and then combine all aligned EEG trials from the source subjects into a single source domain.

For a subject with N EEG trials $\{X^n\}_{n=1}^N$, EA

Table 2. Average semi-supervised cross-species and within-modality transfer AUCs (%) on Kaggle and Freiburg iEEG datasets, with increasing amount of labeled data from the target species. The best average AUC of each task is marked in bold, and the second best by an underline.

Approach		Canine (iEEG, Kaggle) to Human (iEEG, Kaggle)					Human (iEEG, Kaggle) to Canine (iEEG, Kaggle)				
		5%	10%	15%	20%	Avg.	5%	10%	15%	20%	Avg.
Baseline	Within ¹	66.28 \pm 2.5	72.18 \pm 1.0	77.81 \pm 1.2	79.20 \pm 1.0	73.87	74.08 \pm 1.0	77.78 \pm 3.1	84.05 \pm 1.0	87.34 \pm 1.3	80.81
	Comb. ²	83.34 \pm 0.4	87.99 \pm 0.5	91.27 \pm 0.5	91.90 \pm 0.8	88.63	83.12 \pm 2.1	87.46 \pm 1.0	90.32 \pm 2.8	93.37 \pm 3.2	88.57
	DAN	81.96 \pm 0.6	88.01 \pm 0.6	87.32 \pm 0.9	89.90 \pm 1.1	86.80	84.29 \pm 1.6	85.97 \pm 2.6	91.64 \pm 0.9	94.69 \pm 1.1	89.15
	JAN	81.34 \pm 1.1	86.79 \pm 1.0	88.52 \pm 0.2	89.69 \pm 0.5	86.59	83.43 \pm 0.8	87.37 \pm 2.6	92.30 \pm 1.5	93.85 \pm 1.7	89.24
	SHOT	85.41 \pm 1.6	86.97 \pm 1.4	89.13 \pm 0.9	90.90 \pm 0.6	88.10	82.50 \pm 1.5	87.14 \pm 1.0	90.70 \pm 0.5	91.94 \pm 0.3	88.07
	DSAN	81.76 \pm 0.9	84.73 \pm 0.6	86.66 \pm 1.0	86.94 \pm 0.8	85.02	81.58 \pm 1.7	86.12 \pm 2.0	91.61 \pm 0.7	94.09 \pm 1.6	88.35
	MCC	86.64 \pm 2.0	91.52 \pm 0.9	91.50 \pm 1.0	93.31 \pm 0.5	90.74	89.37 \pm 1.2	90.52 \pm 0.1	93.30 \pm 1.0	95.37 \pm 0.8	92.14
ResizeNet+	AT	89.29 \pm 0.6	92.68 \pm 0.5	94.09 \pm 0.5	<u>95.88</u> \pm 0.3	92.99	86.16 \pm 1.2	91.05 \pm 0.9	94.22 \pm 0.5	<u>97.34</u> \pm 0.7	92.19
	NST	88.72 \pm 1.0	91.43 \pm 0.7	94.13 \pm 0.5	94.76 \pm 0.5	92.26	85.24 \pm 1.3	90.13 \pm 2.1	92.17 \pm 1.4	94.18 \pm 1.1	90.43
	SP	<u>90.31</u> \pm 0.2	<u>93.08</u> \pm 0.7	<u>94.52</u> \pm 0.7	95.64 \pm 0.0	<u>93.39</u>	86.61 \pm 1.1	91.22 \pm 0.6	94.79 \pm 1.5	96.84 \pm 0.6	92.37
	RKD	88.55 \pm 0.6	91.52 \pm 0.6	92.49 \pm 0.0	94.19 \pm 0.5	91.69	85.97 \pm 0.5	90.02 \pm 1.8	92.22 \pm 1.8	92.86 \pm 1.7	90.27
	PKT	89.26 \pm 0.7	92.63 \pm 0.7	94.10 \pm 0.4	96.12 \pm 0.6	93.03	85.81 \pm 0.5	90.38 \pm 1.7	95.12 \pm 1.2	97.96 \pm 0.3	92.32
	CC	88.32 \pm 2.2	93.16 \pm 0.4	94.08 \pm 0.5	95.65 \pm 0.5	92.80	87.19 \pm 0.9	<u>92.09</u> \pm 0.4	<u>95.33</u> \pm 0.1	95.74 \pm 0.0	<u>92.59</u>
	MSA (ours)	91.10 \pm 1.0	92.90 \pm 0.1	94.78 \pm 0.1	95.75 \pm 0.1	93.63	<u>88.44</u> \pm 0.4	92.93 \pm 0.1	95.59 \pm 0.8	96.72 \pm 0.9	93.42
Approach		Canine (iEEG, Kaggle) to Human (iEEG, Freiburg)					Human (iEEG, Freiburg) to Canine (iEEG, Kaggle)				
		5%	10%	15%	20%	Avg.	5%	10%	15%	20%	Avg.
Baseline	Within	62.13 \pm 0.5	67.33 \pm 0.2	72.00 \pm 1.2	73.94 \pm 0.6	68.85	74.08 \pm 1.0	77.78 \pm 3.1	84.05 \pm 1.0	87.34 \pm 1.3	80.81
	Comb.	83.86 \pm 2.5	84.62 \pm 0.3	85.84 \pm 0.8	85.61 \pm 0.6	84.98	87.03 \pm 0.4	92.98 \pm 0.4	95.47 \pm 0.7	96.15 \pm 0.3	92.91
	DAN	<u>89.81</u> \pm 1.3	<u>92.45</u> \pm 0.9	<u>93.16</u> \pm 1.2	<u>93.44</u> \pm 0.7	<u>92.22</u>	85.26 \pm 1.7	89.42 \pm 1.7	93.68 \pm 0.4	93.73 \pm 0.5	90.52
	JAN	86.47 \pm 1.3	89.65 \pm 0.3	89.28 \pm 0.1	90.81 \pm 0.5	89.05	85.71 \pm 0.3	90.12 \pm 0.2	94.57 \pm 0.4	94.79 \pm 0.6	91.30
	SHOT	79.13 \pm 0.4	82.49 \pm 0.7	85.20 \pm 0.6	84.60 \pm 1.0	82.86	88.37 \pm 1.1	91.55 \pm 0.4	94.17 \pm 0.6	94.76 \pm 0.4	92.21
	DSAN	84.87 \pm 3.0	86.42 \pm 1.5	86.22 \pm 2.0	88.70 \pm 1.4	86.55	80.52 \pm 0.6	85.84 \pm 1.1	89.95 \pm 1.6	88.19 \pm 2.8	86.13
	MCC	85.69 \pm 0.8	86.59 \pm 1.0	86.96 \pm 0.5	87.79 \pm 0.8	86.76	90.69 \pm 0.6	<u>95.93</u> \pm 0.4	96.50 \pm 0.3	97.29 \pm 0.7	<u>95.10</u>
ResizeNet+	AT	86.35 \pm 1.1	89.07 \pm 0.7	89.07 \pm 0.5	89.38 \pm 0.2	88.47	89.29 \pm 4.3	94.58 \pm 0.4	96.50 \pm 0.9	96.91 \pm 0.8	94.32
	NST	84.55 \pm 1.7	86.38 \pm 1.1	87.32 \pm 2.1	87.95 \pm 2.3	86.55	88.17 \pm 4.1	88.88 \pm 3.3	93.74 \pm 1.9	93.78 \pm 2.7	91.14
	SP	86.40 \pm 1.6	89.73 \pm 0.6	89.25 \pm 1.1	89.66 \pm 0.4	88.76	90.97 \pm 3.0	92.47 \pm 0.8	96.23 \pm 1.1	<u>97.53</u> \pm 0.1	94.30
	RKD	82.84 \pm 1.8	88.06 \pm 1.0	87.68 \pm 2.2	88.99 \pm 2.1	86.89	88.84 \pm 1.7	93.48 \pm 2.3	<u>96.90</u> \pm 0.2	97.21 \pm 0.4	94.11
	PKT	86.47 \pm 1.2	89.65 \pm 0.3	89.15 \pm 0.0	90.77 \pm 0.5	89.01	<u>91.59</u> \pm 2.3	94.37 \pm 1.1	96.84 \pm 1.2	97.32 \pm 0.2	95.03
	CC	86.12 \pm 0.6	89.32 \pm 0.6	89.57 \pm 0.2	90.43 \pm 0.7	88.86	89.53 \pm 3.9	92.95 \pm 2.0	96.33 \pm 0.2	96.94 \pm 0.6	93.94
	MSA (ours)	91.06 \pm 0.9	93.90 \pm 1.2	94.78 \pm 1.0	94.79 \pm 0.8	93.63	92.85 \pm 0.5	96.92 \pm 0.9	97.04 \pm 0.6	97.92 \pm 0.1	96.18

¹ Within: This baseline trains the model solely on the $l\%$ labeled iEEG data of the current species, without utilizing any labeled iEEG data from other species.

² Comb.: Train the model on the combination of $l\%$ labeled iEEG data from the current species and all labeled iEEG data from the other species, without employing any alignment strategies.

Table 3. Average semi-supervised cross-species transfer AUCs (%) on CHSZ and NICU sEEG datasets. The best average AUC of each task is marked in bold, and the second best by an underline.

Approach		Canine (iEEG, Kaggle) to Human (sEEG, CHSZ)					Human (sEEG, CHSZ) to Canine (iEEG, Kaggle)				
		5%	10%	15%	20%	Avg.	5%	10%	15%	20%	Avg.
Baseline	Within	62.02 \pm 0.6	64.02 \pm 0.2	65.65 \pm 1.2	70.14 \pm 1.6	65.46	74.08 \pm 1.0	77.78 \pm 3.1	84.05 \pm 1.0	87.34 \pm 1.3	80.81
	Comb.	78.97 \pm 1.4	80.24 \pm 0.9	80.09 \pm 2.4	79.93 \pm 2.3	79.81	83.84 \pm 0.7	89.64 \pm 0.4	91.31 \pm 0.5	93.60 \pm 0.9	89.60
	DAN	74.24 \pm 0.8	74.28 \pm 1.8	76.43 \pm 1.0	75.36 \pm 2.5	75.08	84.05 \pm 0.2	90.48 \pm 0.3	<u>92.89</u> \pm 1.0	<u>94.28</u> \pm 0.9	90.43
	JAN	70.10 \pm 2.0	69.03 \pm 1.0	71.23 \pm 0.9	72.16 \pm 1.2	70.63	76.83 \pm 0.0	82.32 \pm 1.4	86.56 \pm 3.4	89.53 \pm 3.1	83.81
	SHOT	72.96 \pm 2.2	73.20 \pm 0.8	73.64 \pm 1.7	74.48 \pm 1.5	73.57	79.74 \pm 1.8	86.95 \pm 0.0	88.84 \pm 0.8	89.47 \pm 1.1	86.25
	DSAN	68.34 \pm 1.1	70.86 \pm 1.2	70.12 \pm 0.5	71.79 \pm 1.9	70.28	82.12 \pm 1.0	86.72 \pm 6.7	88.15 \pm 1.1	88.86 \pm 0.3	86.46
	MCC	76.32 \pm 1.5	78.44 \pm 0.5	78.68 \pm 1.0	78.60 \pm 1.4	78.01	83.54 \pm 2.0	89.73 \pm 1.2	92.36 \pm 0.8	93.56 \pm 0.8	89.80
ResizeNet+	AT	85.00 \pm 1.3	85.87 \pm 0.9	87.83 \pm 0.5	88.11 \pm 0.7	86.70	82.99 \pm 1.5	85.70 \pm 1.3	89.99 \pm 1.3	89.84 \pm 0.9	87.13
	NST	83.71 \pm 0.8	83.85 \pm 1.7	86.64 \pm 0.1	88.45 \pm 1.0	85.66	<u>85.35</u> \pm 1.8	<u>91.19</u> \pm 0.6	92.39 \pm 1.0	93.70 \pm 1.5	<u>90.66</u>
	SP	83.35 \pm 2.2	86.51 \pm 0.3	<u>88.26</u> \pm 0.8	<u>88.69</u> \pm 0.5	86.70	82.31 \pm 2.6	87.50 \pm 1.5	90.30 \pm 1.5	93.01 \pm 1.1	88.28
	RKD	84.46 \pm 1.0	85.25 \pm 2.0	86.19 \pm 0.4	87.94 \pm 0.4	85.96	84.27 \pm 4.3	88.79 \pm 1.2	86.93 \pm 1.1	92.74 \pm 1.2	88.18
	PKT	86.40 \pm 0.4	<u>86.25</u> \pm 0.5	87.36 \pm 0.8	89.19 \pm 0.5	87.30	83.29 \pm 2.3	87.36 \pm 1.6	89.80 \pm 1.5	92.92 \pm 1.2	88.34
	CC	84.35 \pm 1.9	85.64 \pm 2.1	88.63 \pm 1.4	88.35 \pm 0.7	<u>86.74</u>	85.20 \pm 2.2	89.57 \pm 0.8	90.92 \pm 1.0	92.60 \pm 1.7	89.57
	MSA (ours)	82.74 \pm 1.9	84.14 \pm 1.8	84.84 \pm 0.6	86.02 \pm 1.2	84.44	86.96 \pm 1.5	91.22 \pm 1.9	94.93 \pm 2.3	94.79 \pm 1.9	91.98
Approach		Canine (iEEG, Kaggle) to Human (sEEG, NICU)					Human (sEEG, NICU) to Canine (iEEG, Kaggle)				
		5%	10%	15%	20%	Avg.	5%	10%	15%	20%	Avg.
Baseline	Within	62.13 \pm 0.5	67.33 \pm 0.2	72.00 \pm 1.2	73.94 \pm 0.6	68.85	74.08 \pm 1.0	77.78 \pm 3.1	84.05 \pm 1.0	87.34 \pm 1.3	80.81
	Comb.	71.01 \pm 0.7	74.01 \pm 0.3	76.51 \pm 0.2	78.90 \pm 0.7	75.11	84.82 \pm 0.7	85.88 \pm 1.6	87.02 \pm 2.8	92.08 \pm 1.0	87.45
	DAN	70.37 \pm 0.3	73.45 \pm 0.5	75.57 \pm 0.4	77.82 \pm 1.0	74.30	<u>88.94</u> \pm 1.4	<u>94.27</u> \pm 1.0	92.44 \pm 1.8	94.52 \pm 1.3	92.54
	JAN	67.90 \pm 1.1	71.23 \pm 0.7	74.28 \pm 0.3	75.26 \pm 0.5	72.17	84.05 \pm 0.4	92.31 \pm 0.1	93.19 \pm 0.7	94.14 \pm 1.0	90.92
	SHOT	65.18 \pm 1.4	69.57 \pm 1.2	73.06 \pm 0.2	73.80 \pm 0.3	70.40	77.74 \pm 1.0	86.17 \pm 0.8	88.65 \pm 1.7	89.80 \pm 1.7	85.59
	DSAN	66.44 \pm 0.7	70.63 \pm 0.2	71.03 \pm 1.0	72.76 \pm 0.2	70.22	75.26 \pm 2.0	85.57 \pm 1.4	87.36 \pm 1.7	82.20 \pm 3.3	82.60
	MCC	66.18 \pm 0.4	71.33 \pm 0.9	74.75 \pm 1.2	77.01 \pm 0.1	72.32	83.55 \pm 0.5	92.21 \pm 0.8	94.44 \pm 0.5	<u>95.67</u> \pm 0.9	91.47
ResizeNet+	AT	74.28 \pm 2.6	<u>77.87</u> \pm 2.6	79.12 \pm 2.5	<u>81.17</u> \pm 3.0	<u>78.11</u>	85.11 \pm 0.5	91.22 \pm 0.8	91.75 \pm 1.8	92.79 \pm 1.6	90.22
	NST	70.61 \pm 0.9	72.70 \pm 1.6	75.60 \pm 1.5	76.42 \pm 1.7	73.83	90.08 \pm 1.3	94.34 \pm 1.5	<u>94.92</u> \pm 1.2	94.74 \pm 1.7	93.52
	SP	74.54 \pm 0.6	76.90 \pm 1.5	78.17 \pm 1.9	80.77 \pm 2.6	77.60	85.29 \pm 0.8	89.57 \pm 0.4	91.42 \pm 1.8	93.04 \pm 2.6	89.83
	RKD	72.13 \pm 0.8	76.74 \pm 0.7	76.18 \pm 0.8	79.35 \pm 1.2	76.10	84.26 \pm 2.4	86.85 \pm 0.4	90.67 \pm 0.7	91.87 \pm 1.4	88.41
	PKT	<u>75.21</u> \pm 0.8	77.46 \pm 1.8	78.82 \pm 1.5	80.57 \pm 2.7	78.02	84.53 \pm 0.1	91.95 \pm 1.9	91.35 \pm 0.1	92.23 \pm 1.8	90.02
	CC	73.51 \pm 3.1	74.24 \pm 2.6	<u>79.66</u> \pm 0.7	80.26 \pm 2.4	76.92	86.55 \pm 1.0	90.84 \pm 2.1	95.40 \pm 0.2	94.60 \pm 0.5	91.85
	MSA (ours)	75.48 \pm 0.5	79.07 \pm 0.4	82.56 \pm 0.7	84.33 \pm 0.2	80.36	88.03 \pm 1.3	93.87 \pm 1.4	93.91 \pm 3.0	96.21 \pm 1.1	<u>93.01</u>

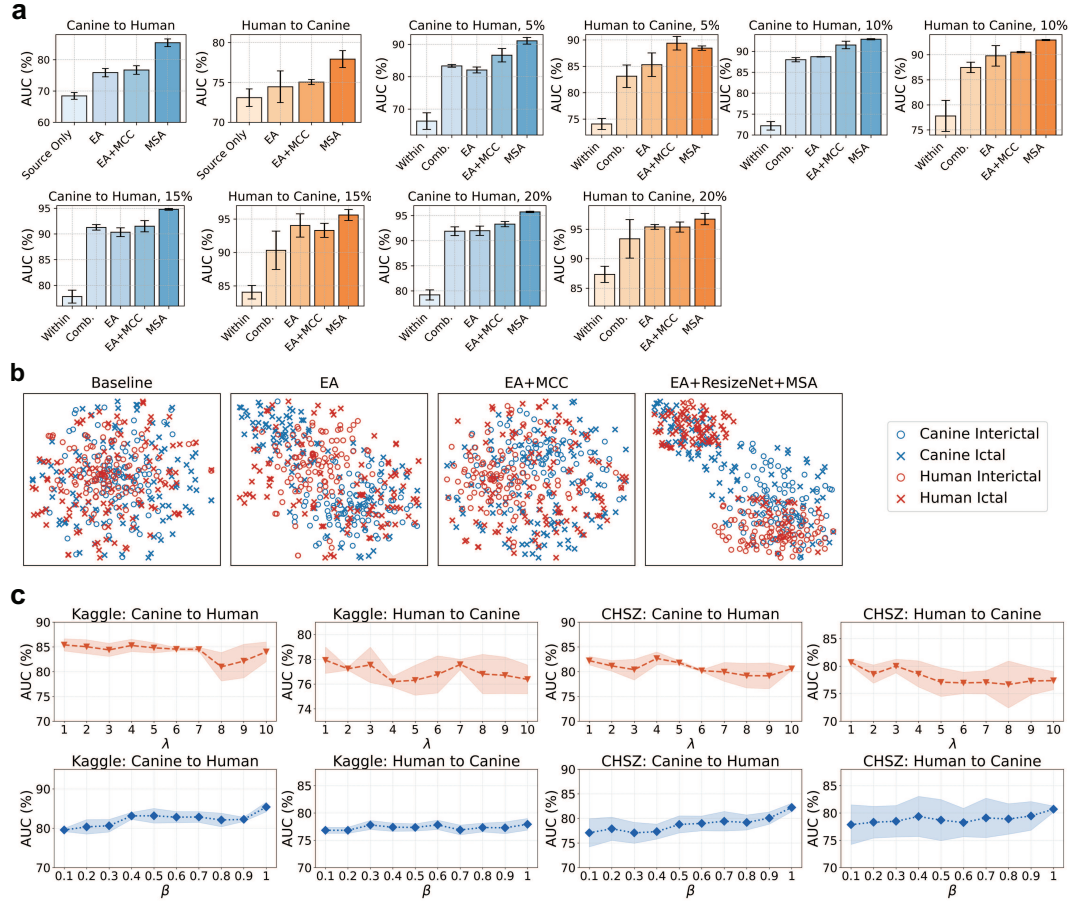


Figure 2. Ablation study, t -SNE feature visualization, and parameter sensitivity analysis. **a**, Ablation study on the Kaggle iEEG dataset, including two tasks of canine-to-human and human-to-canine, and two scenarios of unsupervised cross-species transfer and semi-supervised cross-species transfer. **b**, Feature t -SNE visualizations on the Kaggle iEEG data. **c**, Parameter sensitivity analysis of λ and β on the Kaggle iEEG dataset and CHSZ sEEG dataset using the proposed ResizeNet+MSA approach. A point denotes the average, and the shadow denotes the standard deviation.

first computes their mean covariance matrix:

$$\bar{R} = \frac{1}{N} \sum_{n=1}^N X^n (X^n)^\top, \quad (1)$$

and then performs the alignment by

$$\tilde{X}^n = \bar{R}^{-1/2} X^n. \quad (2)$$

\tilde{X}^n then replaces X^n in all subsequent operations.

This process is repeated for each subject in the source and target species to normalize its mean covariance matrix to the identity matrix, making them more consistent.

Input space alignment

As illustrated in Figure A1b, addressing the disparity in channel dimensionality is pivotal to effective cross-species transfer. Our proposed solution combines a Transformer Encoder with a

linear layer in a neural network architecture, referred to as ResizeNet.

The Transformer Encoder captures the intricate temporal dependencies and spatial relationships in the EEG data, reflecting the interconnections between distinct channel locations using a self-attention mechanism. Subsequently, a linear layer is employed to project EEG data from a higher dimensionality to a lower space, ensuring consistent input to the subsequent feature extractor.

Let the original EEG data be represented as $X \in \mathbb{R}^{N \times C \times T_s}$, where N is the training batch size, C the number of channels, and T_s the number of time samples. The EEG data are first reshaped to $X \in \mathbb{R}^{N \times T_s \times C}$, and then input to the Transformer Encoder, which includes multi-head self-attention and a feedforward neural network. After this, a linear layer reduces the dimensionality for species with more channels. For instance, the human sEEG data in the CHSZ dataset have 18 channels, whereas the canine

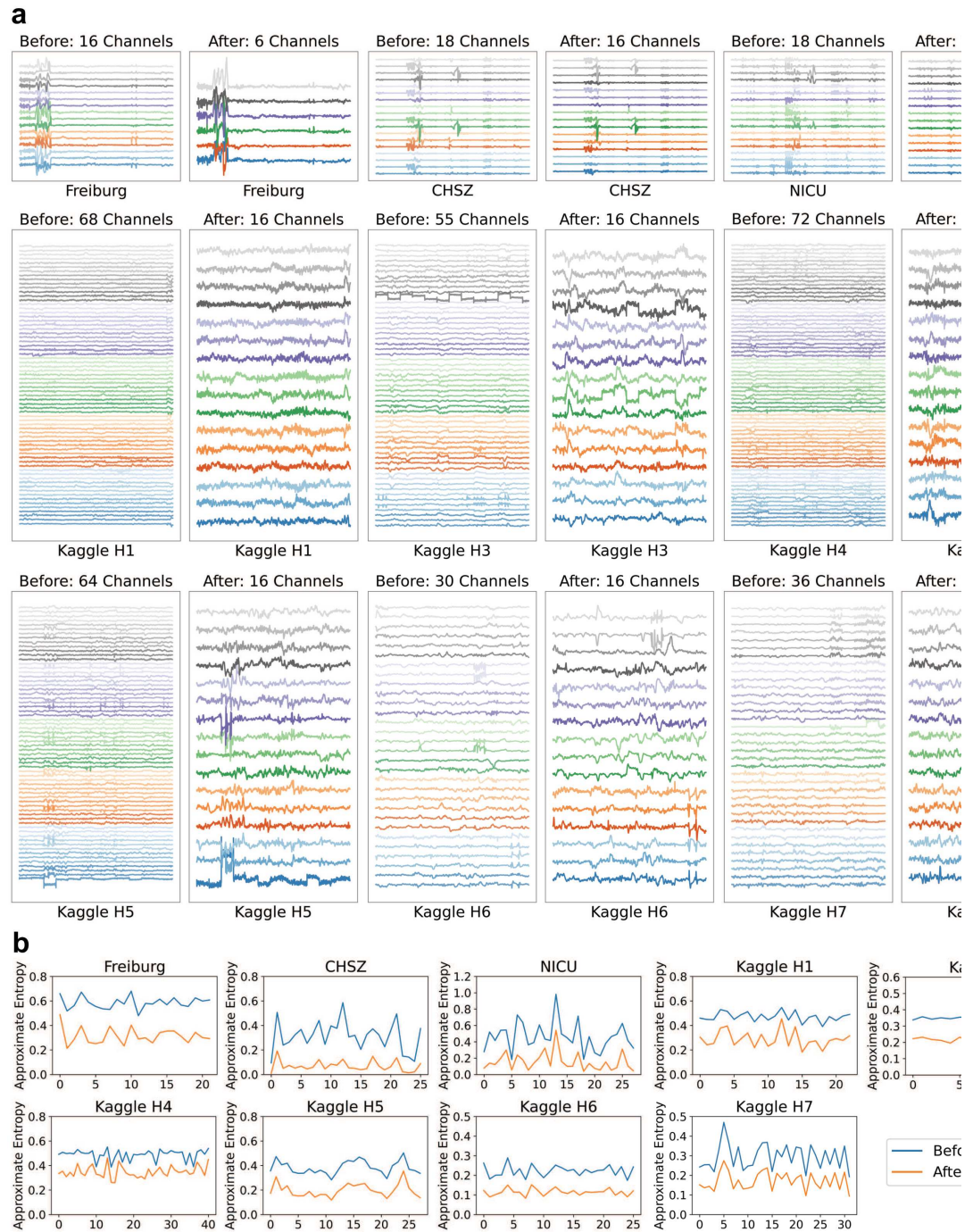


Figure 3. Effect of input space alignment via the proposed ResizeNet on the four datasets. **a**, The iEEG/sEEG signals before and after ResizeNet exhibit similar temporal structures, demonstrating the effectiveness of ResizeNet. ResizeNet unifies the number of channels from different species, accommodating the input space discrepancies while preserving critical temporal structures and features. **b**, Mean approximate entropy of all channels before and after ResizeNet on the four datasets, showing that ResizeNet preserves important entropy features of the iEEG/sEEG signals.

iEEG data in the Kaggle dataset have 16 channels; when transferring from the CHSZ dataset to the Kaggle dataset, ResizeNet reduces the human sEEG data to 16 channels to match the dimensionality of the canine iEEG data.

The final ResizeNet transformation is expressed as:

$$\hat{X} = R(T(R(X)) \cdot W_L), \quad (3)$$

where $R(\cdot)$ is the reshape function used for switching the last two dimensions of data, $T(\cdot)$ the Transformer Encoder with two layers and two heads, and $W_L \in \mathbb{R}^{C \times C_t}$ the learned parameter matrix, with C_t being the target number of channels.

Feature space alignment

After ResizeNet alignment that unifies the input signal dimensionality from both source and target species, domain adaptation can then be conducted to further align the feature distributions.

Domain adaptation leverages data from the labeled source domain $\mathcal{D}_s = \{(\mathbf{X}_s^i, y_s^i)\}_{i=1}^{N_s}$ and the unlabeled target domain $\mathcal{D}_t = \{(\mathbf{X}_t^i)\}_{i=1}^{N_t}$ to minimize their discrepancies, enabling the model trained on the source domain to generalize to the target domain. Traditional domain adaptation methods mainly consider the simpler homogeneous domain adaptation, i.e., the feature spaces of the source and target domains are identical ($\mathcal{X}_s = \mathcal{X}_t$), but their probability distributions are different ($P(X_s, y_s) \neq P(X_t, y_t)$).

The loss function of domain adaptation using MMD is:

$$L_{DA} = \text{MMD}^2(X_s, \hat{X}_t) = \left\| \frac{1}{N_s} \sum_{i=1}^{N_s} \phi(x_i^s) - \frac{1}{N_t} \sum_{j=1}^{N_t} \phi(\hat{x}_j^t) \right\|_{\mathcal{H}}^2, \quad (4)$$

where \mathcal{H} is a reproducing kernel Hilbert space with a feature mapping ϕ . Extensions of MMD, e.g., joint MMD [36] and local MMD [37], can also be utilized in domain adaptation regularization.

Output space alignment

We utilize knowledge distillation to further align the output spaces. Knowledge distillation forces the student model to mimic the teacher model's behavior by imposing a stringent congruent constraint on their predictions, typically utilizing the Kullback–Leibler divergence.

As illustrated in Figure A1c, the original EEG signals with C channels are first reduced to C_t channels by ResizeNet, or through simple channel selection (the first C_t channels were used in this paper). In this way, we obtain two different signals with the same shape, one by ResizeNet and the other by channel selection. A neural network is then used to compute z_r , the logits from ResizeNet, and z_s , the logits from channel selection. Subsequently, knowledge distillation is performed on z_r and z_s :

$$L_{KD} = \frac{1}{N} \sum_{i=1}^N \tau^2 KL(p_r^\tau, p_s^\tau), \quad (5)$$

where τ is a relaxation parameter (referred as the temperature in [31]) to soften the output of the teacher network, and $p^\tau = \frac{\exp(z_i/\tau)}{\sum_j \exp(z_j/\tau)}$ is the softmax operation, with z_i being the logit for the i -th class.

Multi-space alignment

To minimize the gaps between species, we perform the above input-space, feature-space, and output-space alignments simultaneously. In the proposed cross-species transfer learning framework shown in Figure A1a, we first perform EA and ResizeNet to match the input dimensionality of the source and target species. Then, domain adaptation is performed to further reduce the discrepancies in the feature space. Finally, knowledge distillation is performed on the logits from ResizeNet and channel selection strategy.

The overall optimization objective is composed of three parts: the supervised cross-entropy loss, the domain adaptation loss, and the knowledge distillation loss:

$$L = L_{CE} + \lambda \cdot L_{KD} + \beta \cdot L_{DA}, \quad (6)$$

where L_{CE} is the classic cross-entropy loss for supervised learning, and λ and β are trade-off hyperparameters.

To summarize, EA normalizes all data in the input space to a similar scale, ResizeNet projects higher dimensional data to a lower dimensionality, domain adaptation further aligns the feature distributions, and knowledge distillation finally aligns the model predictions.

Implementation details

EEGNet [38], a popular end-to-end convolutional neural network for EEG signal decoding, was utilized as the feature extractor, along with

a fully connected layer as the classifier. In unsupervised cross-species transfer, all data from the target species were unlabeled for testing. In semi-supervised cross-species transfer, the first $l\%$ labeled data of all subjects from the target species were combined and utilized during training, and the remaining $(100 - l)\%$ were used for testing. The trade-off parameters λ and β were both set to 1 in all experiments. To avoid temporal leakage pointed out in previous works [39], we partitioned the training and test data from the target species chronologically instead of randomly.

All experiments were repeated three times, and the average results are reported. All algorithms were implemented in PyTorch.

REFERENCES

1. Wang C, Sun W, Zhang J *et al.* An electric-field-responsive paramagnetic contrast agent enhances the visualization of epileptic foci in mouse models of drug-resistant epilepsy. *Nature Biomedical Engineering* 2021; **5**: 278–289.
2. Bui AD, Nguyen TM, Limouse C *et al.* Dentate gyrus mossy cells control spontaneous convulsive seizures and spatial memory. *Science* 2018; **359**: 787–790.
3. Karoly PJ, Rao VR, Gregg NM *et al.* Cycles in epilepsy. *Nature Reviews Neurology* 2021; **17**: 267–284.
4. Téllez-Zenteno JF, Dhar R, Hernandez-Ronquillo L *et al.* Long-term outcomes in epilepsy surgery: antiepileptic drugs, mortality, cognitive and psychosocial aspects. *Brain* 2007; **130**: 334–345.
5. Kerr MP. The impact of epilepsy on patients' lives. *Acta Neurologica Scandinavica* 2012; **126**: 1–9.
6. Wang X, Wang Y, Liu D *et al.* Automated recognition of epilepsy from EEG signals using a combining space-time algorithm of CNN-LSTM. *Scientific Reports* 2023; **13**: 14876.
7. Saab K, Dunnmon J, Ré C *et al.* Weak supervision as an efficient approach for automated seizure detection in electroencephalography. *NPJ Digital Medicine* 2020; **3**: 59.
8. Parvizi J and Kastner S. Human intracranial EEG: promises and limitations. *Nature Neuroscience* 2018; **21**: 474.
9. Ney JP, van der Goes DN, Nuwer MR *et al.* Continuous and routine EEG in intensive care: utilization and outcomes, United States 2005–2009. *Neurology* 2013; **81**: 2002–2008.
10. Acharya UR, Sree SV, Swapna G *et al.* Automated EEG analysis of epilepsy: a review. *Knowledge-Based Systems* 2013; **45**: 147–165.
11. Faust O, Acharya UR, Adeli H *et al.* Wavelet-based EEG processing for computer-aided seizure detection and epilepsy diagnosis. *Seizure* 2015; **26**: 56–64.
12. Acharya UR, Fujita H, Sudarshan VK *et al.* Application of entropies for automated diagnosis of epilepsy using EEG signals: A review. *Knowledge-Based Systems* 2015; **88**: 85–96.
13. Acharya UR, Oh SL, Hagiwara Y *et al.* Deep convolutional neural network for the automated detection and diagnosis of seizure using EEG signals. *Computers in Biology and Medicine* 2018; **100**: 270–278.
14. Hussein R, Palangi H, Ward RK *et al.* Optimized deep neural network architecture for robust detection of epileptic seizures using EEG signals. *Clinical Neurophysiology* 2019; **130**: 25–37.
15. Sun Y, Jin W, Si X *et al.* Continuous seizure detection based on Transformer and long-term iEEG. *IEEE Journal of Biomedical and Health Informatics* 2022; **26**: 5418–5427.
16. Wang Z, Zhang W, Li S *et al.* Unsupervised domain adaptation for cross-patient seizure classification. *Journal of Neural Engineering* 2023; **20**: 066002.
17. Rukhsar S and Tiwari AK. Lightweight convolution transformer for cross-patient seizure detection in multi-channel EEG signals. *Computer Methods and Programs in Biomedicine* 2023; **242**: 107856.
18. Zhang Z, Ji T, Xiao M *et al.* Cross-patient automatic epileptic seizure detection using patient-adversarial neural networks with spatio-temporal EEG augmentation. *Biomedical Signal Processing and Control* 2024; **89**: 105664.
19. Chen ZP, Wang S, Zhao X *et al.* Lipid-accumulated reactive astrocytes promote disease progression in epilepsy. *Nature Neuroscience* 2023; **26**: 542–554.
20. Devinsky O, Boesch JM, Cerda-Gonzalez S *et al.* A cross-species approach to disorders affecting brain and behaviour. *Nature Reviews Neurology* 2018; **14**: 677–686.
21. Wang Y and Cai Y. Obtaining human ischemic stroke gene expression biomarkers from animal models: a cross-species validation study. *Scientific Reports* 2016; **6**: 29693.
22. Chan F, Lax NZ, Voss CM *et al.* The role of astrocytes in seizure generation: insights from a novel in vitro seizure model based on mitochondrial dysfunction. *Brain* 2019; **142**: 391–411.
23. Berendt M, Høgenhaven H, Flagstad A *et al.* Electroencephalography in dogs with epilepsy: similarities between human and canine findings. *Acta Neurologica Scandinavica* 1999; **99**: 276–283.
24. Chandler K. Canine epilepsy: what can we learn from human seizure disorders? *The Veterinary Journal* 2006; **172**: 207–217.
25. Holliday T, Cunningham J and Gutnick M. Comparative clinical and electroencephalographic studies of canine epilepsy. *Epilepsia* 1970; **11**: 281–292.
26. Baldassano SN, Brinkmann BH, Ung H *et al.* Crowdsourcing seizure detection: algorithm development and validation on human implanted device recordings. *Brain* 2017; **140**: 1680–1691.
27. Ihle M, Feldwisch-Drentrup H, Teixeira CA *et al.* EPILEPSIAE—A European epilepsy database. *Computer Methods and Programs in Biomedicine* 2012; **106**: 127–138.
28. Stevenson NJ, Tapani K, Lauronen L *et al.* A dataset of neonatal EEG recordings with seizure annotations. *Scientific Data* 2019; **6**: 1–8.
29. He H and Wu D. Transfer learning for brain-computer interfaces: A Euclidean space data alignment approach. *IEEE Trans. on Biomedical Engineering* 2020; **67**: 399–410.
30. Wilson G and Cook DJ. A survey of unsupervised deep domain adaptation. *ACM Trans. on Intelligent Systems and Technology* 2020; **11**: 1–46.
31. Hinton G, Vinyals O and Dean J. Distilling the knowledge in a neural network 2015.
32. Van der Maaten L and Hinton G. Visualizing data using t-SNE. *Journal of Machine Learning Research* 2008; **9**: 2579–2605.

33. Wu D, Jiang X and Peng R. Transfer learning for motor imagery based brain-computer interfaces: A tutorial. *Neural Networks* 2022; **153**: 235–253.
34. Junqueira B, Aristimunha B, Chevallier S *et al.* A systematic evaluation of euclidean alignment with deep learning for EEG decoding. *Journal of Neural Engineering* 2024; **21**: 036038.
35. Wu D, Lu BL, Hu B *et al.* Affective brain-computer interfaces (abcis): A tutorial. *Proceedings of the IEEE* 2023; **111**: 1314–1332.
36. Long M, Zhu H, Wang J *et al.* Deep transfer learning with joint adaptation networks 2017.
37. Zhu Y, Zhuang F, Wang J *et al.* Deep subdomain adaptation network for image classification. *IEEE Trans. on Neural Networks and Learning Systems* 2020; **32**: 1713–1722.
38. Lawhern VJ, Solon AJ, Waytowich NR *et al.* EEGNet: A compact convolutional neural network for EEG-based brain-computer interfaces. *Journal of Neural Engineering* 2018; **15**: 056013.
39. Kapoor S and Narayanan A. Leakage and the reproducibility crisis in machine-learning-based science. *Patterns* 2023; **4**: 100804.
40. Long M, Cao Y, Wang J *et al.* Learning transferable features with deep adaptation networks 2015.
41. Gretton A, Borgwardt KM, Rasch MJ *et al.* A kernel two-sample test. *Journal of Machine Learning Research* 2012; **13**: 723–773.
42. Jin Y, Wang X, Long M *et al.* Minimum class confusion for versatile domain adaptation 2020.
43. Liang J, Hu D, Wang Y *et al.* Source data-absent unsupervised domain adaptation through hypothesis transfer and labeling transfer. *IEEE Trans. Pattern Analysis and Machine Intelligence* 2022; **44**: 8602–8617.
44. Zagoruyko S and Komodakis N. Paying more attention to attention: Improving the performance of convolutional neural networks via attention transfer 2017.
45. Huang Z and Wang N. Like what you like: Knowledge distill via neuron selectivity transfer. *arXiv preprint arXiv:1707.01219* 2017; .
46. Tung F and Mori G. Similarity-preserving knowledge distillation 2019.
47. Park W, Kim D, Lu Y *et al.* Relational knowledge distillation 2019.
48. Passalis N and Tefas A. Learning deep representations with probabilistic knowledge transfer 2018.
49. Peng B, Jin X, Liu J *et al.* Correlation congruence for knowledge distillation 2019.

APPENDIX A: COMPARED APPROACHES

The proposed multi-space alignment method is presented in Figure A1.

Five popular unsupervised domain adaptation approaches were compared:

1. Deep Adaptation Network (DAN) [40], which achieves feature alignment by minimizing the maximum mean discrepancies (MMD) [41] in the feature space.
2. Joint Adaptation Network (JAN) [36] and Deep Subdomain Adaptation Network (DSAN) [37], which construct transfer networks by aligning class-conditioned subdomain distributions based on local MMD in the feature space, utilizing either model prediction probabilities or pseudo-labels.
3. Minimum class confusion (MCC) [42], which integrates a weighted prediction entropy with class correlation to reduce class confusion in the output space.
4. Source hypothesis transfer (SHOT) [43], which utilizes information maximization for conditional entropy minimization and label marginal entropy regularization in the output space.

Six popular and diverse knowledge distillation approaches were combined with the proposed ResizeNet to further improve the alignment performance:

1. Attention Transfer (AT) [44], which utilizes an attention mechanism to enhance the student network's performance by mapping attention from the teacher's feature maps.
2. Neuron Selectivity Transfer (NST) [45], which treats knowledge transfer as a distribution matching problem by aligning neuron selectivity patterns between networks.
3. Similarity-Preserving (SP) [46], which ensures the preservation of pairwise similarities between activations in the teacher network to maintain relational integrity in the student network.
4. Relational Knowledge Distillation (RKD) [47], which focuses on transferring mutual relations of data samples using distance-wise and angle-wise distillation losses.
5. Probabilistic Knowledge Transfer (PKT) [48], which aligns the probability distributions in the feature space, rather than directly mapping the features.
6. Correlation Congruence (CC) [49], which transfers correlations between instances using a generalized kernel method based on the Taylor series expansion.

APPENDIX B: DATASET INFORMATION

The Kaggle dataset includes data from eight human patients and four canines, provided by the Mayo Clinic and University of Pennsylvania. The canines were continuously monitored via video and iEEG. The iEEG data were acquired from an implanted device with a sampling rate of 400 Hz, utilizing 16 subdural electrodes arranged on two standard, human-sized, 4-contact strips implanted in an anteroposterior position on each hemisphere. The remaining eight human patients had drug-resistant epilepsy and were undergoing iEEG monitoring at Mayo Clinic Rochester. These signals were continuously sampled at either 500 or 5000 Hz, using varying subdural electrode grids based on individual clinical considerations [26].

The Freiburg dataset comprises invasive long-term iEEG recordings from 21 human patients, acquired at a sampling rate of 256 Hz during invasive pre-surgical epilepsy monitoring at the Epilepsy Center of the University Hospital of Freiburg, Germany. The iEEG signals were recorded with three focal and three extra-focal electrode contacts [27].

The CHSZ dataset consists of sEEG recordings from 27 children, aged three months to ten years. The original sampling rate was either 500 Hz or 1000 Hz. Each subject had one to six seizure events. Experts annotated the onset and offset of each seizure for every child [16].

The NICU dataset documented neonatal seizures from 79 full-term neonates, with a sampling frequency of 256 Hz and a median recording duration of 74 minutes (interquartile range: 64 to 96 minutes). Three experts independently annotated each second of sEEG data, yielding an average of 460 seizures per expert. According to their consensus, 39 neonates experienced seizures, and these data were incorporated into our experiments [28].

Table B1 shows the main characteristics of four datasets. Tables B2-B4 provide detailed characteristics for each subject in the Kaggle, Freiburg and CHSZ datasets, respectively.

APPENDIX C: DATA PREPROCESSING

For the NICU and CHSZ datasets, the original sEEG signals were acquired using 19 unipolar electrodes positioned according to the international 10–20 system, from which 18 bipolar channels were derived [16]: Fp2-F4, F4-C4, C4-P4, P4-O2, Fp1-F3, F3-C3, C3-P3, P3-O1, Fp2-F8, F8-T4, T4-T6, T6-O2, Fp1-F7, F7-T3, T3-T5, T5-O1, Fz-Cz, and Cz-Pz.

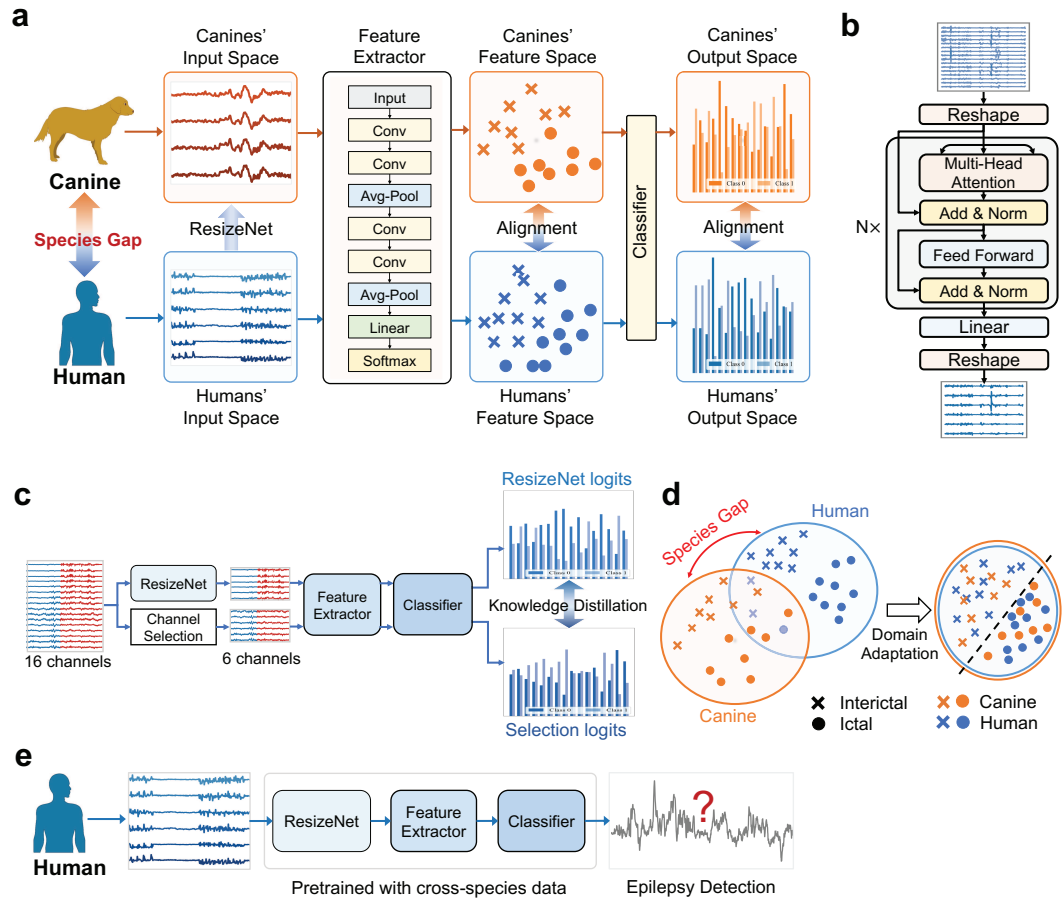


Figure A1. Overview of the proposed cross-species and cross-modality epilepsy seizure detection framework. **a**, Training of the cross-species and cross-modality transfer network utilizes iEEG/sEEG data from both canines and humans. **b**, The proposed ResizeNet, which projects EEG signal of the species with higher dimensionality (collected with more EEG electrodes) to a lower dimensionality to match their feature spaces. **c**, The integration of knowledge distillation with ResizeNet for output-space alignment. **d**, Domain adaptation for distribution matching to achieve feature-space alignment. **e**, Illustration of the test phase on human iEEG/sEEG data.

The EEG signals in all four datasets entered a 50 Hz notch filter and a 0.5-50 Hz bandpass filter, and were then segmented into 1-second non-overlapping trials in the Kaggle and Freiburg datasets, and 4-second trials in the CHSZ and NICU datasets, in line with [16].

In the NICU dataset, EEG segments were independently annotated by three experts on a per-second basis, with groundtruth labels determined by majority consensus. In the other three datasets, a single expert annotated the beginning and end of each seizure. For each cross-species transfer task, the duration of time segments was unified across the source and target species. For instance, when transferring from canines to humans in the Kaggle dataset, the human iEEG signals were downsampled to 400 Hz using the resample function in the MNE package (<https://mne.tools/stable/index.html>).

Table B1. Summary of the four epilepsy datasets

Dataset	EEG Type	# Patients	# Channels	Sampling rate (Hz)	Signal length (second)	# Ictal trials	# Interictal trials
Kaggle	Intracranial	4 canines	16	400	1	1,087	9,116
		8 humans	[16, 72]	500 or 5000	1	1,390	14,329
Freiburg	Intracranial	21 humans	6	256	1	21,000	189,000
NICU	Scalp	39 humans	18	256	4	11,912	40,622
CHSZ	Scalp	27 humans	18	500	4	716	20,521

Table B2. Characteristics of the four canine subjects and eight human subjects in the Kaggle dataset.

Species	ID	# Channels	Sampling rate (Hz)	# Seizures	# Ictal trials	# Interictal trials	# Total trials
Canine	1	16	400	9	178	418	596
	2	16	400	5	172	1,148	1,320
	3	16	400	22	480	4,760	5,240
	4	16	400	6	257	2,790	3,047
Human	1	68	500	7	70	104	174
	2	16	5,000	7	151	2,990	3,141
	3	55	5,000	9	327	714	1,041
	4	72	5,000	5	20	190	210
	5	64	5,000	7	135	2,610	2,745
	6	30	5,000	8	225	2,772	2,997
	7	36	5,000	6	282	3,239	3,521
	8	16	5,000	4	180	1,710	1,890

Table B3. Characteristics of the 21 human subjects in the Freiburg dataset.

ID	Sex	Age	H/NC ¹	Origin of seizure	# Seizures	# Ictal trials	# Interictal trials	# Total trials
1	f	15	NC	Frontal	4	25,200	86,400	111,600
2	m	38	H	Temporal	3	20,243	86,400	106,643
3	m	14	NC	Frontal	5	29,480	86,400	115,880
4	f	26	H	Temporal	5	36,000	86,400	122,400
5	f	16	NC	Frontal	5	35,630	86,400	122,030
6	f	31	H	Temporo/Occipital	3	23,100	86,400	109,500
7	f	42	H	Temporal	3	21,600	88,597	110,197
8	f	32	NC	Frontal	2	12,871	86,979	99,850
9	m	44	NC	Temporo/Occipital	5	36,000	86,163	122,163
10	m	47	H	Temporal	5	38,535	88,047	126,582
11	f	10	NC	Parietal	4	28,800	86,570	115,370
12	f	42	H	Temporal	4	28,800	178,652	207,452
13	f	22	H	Temporo/Occipital	2	14,400	86,400	100,800
14	f	41	H, NC	Fronto/Temporal	4	25,200	85,894	111,094
15	m	31	H, NC	Temporal	4	36,000	86,400	122,400
16	f	50	H	Temporal	5	42,075	86,400	128,475
17	m	28	NC	Temporal	5	53,285	86,634	139,919
18	f	25	NC	Frontal	5	46,698	89,569	136,267
19	f	28	NC	Frontal	4	46,800	87,780	134,580
20	m	33	NC	Temporo/Parietal	5	46,472	92,219	138,691
21	m	13	NC	Temporal	5	43,200	86,177	129,377

¹ H: Hippocampal origin; NC: Neocortical origin.

Table B4. Characteristics of the 27 subjects in the CHSZ dataset.

ID	Age	Seizure subtype ¹	# Seizures	# Ictal trials	# Interictal trials	# Total trials
1	10m	Tonic-Clonic	1	21	170	191
2	7m	Tonic-Clonic	1	13	28	41
3	3m	Tonic-Clonic	1	21	100	121
4	2y1m	Tonic-Clonic	3	11	51	62
5	8y11m	Partial	1	46	16	62
6	4y7m	Tonic-Clonic	1	11	133	144
7	10y10m	Absence	1	10	16	26
8	1y8m	Tonic-Clonic	1	24	13	37
9	1y7m	Tonic-Clonic	1	14	52	66
10	1y8m	Partial	1	50	3,549	3,599
11	1y6m	Partial	4	143	2,595	2,738
12	2y11m	Partial	1	16	3,583	3,599
13	3m	Partial	1	30	224	254
14	3y7m	Absence	6	9	2,560	2,569
15	6y4m	Absence	6	27	158	185
16	3m	Partial	1	33	9	42
17	2y8m	Tonic-Clonic	1	44	53	97
18	3y11m	Absence	3	12	600	612
19	3m	Partial	1	16	1,321	1,337
20	6y3m	Absence	6	16	1,031	1,047
21	6m	Partial	1	23	82	105
22	8y10m	Tonic-Clonic	2	30	36	66
23	8y6m	Partial	4	8	77	85
24	3y10m	Tonic-Clonic	2	33	64	97
25	4y6m	Tonic-Clonic	2	29	89	118
26	7y8m	Partial	1	10	328	338
27	5m	Partial	1	16	3,583	3,599

¹ An expert annotated the beginning and end of each seizure and its subtype (tonic-clonic seizure, absence seizure, or partial seizure) for each child.